Comparative Proteomic Study of Retinal Ganglion Cells Undergoing Various Types of Cellular Stressors.

Christopher R. Starr, James A. Mobley, and Marina S. Gorbatyuk

Department of Optometry and Vision Science, University of Alabama at Birmingham, Birmingham, Alabama, USA, 35233

*To whom correspondence should be addressed:
Dr. Marina S. Gorbatyuk.
Department of Optometry and Vision Science, School of Optometry,
University of Alabama at Birmingham.
1670 University Blvd., Birmingham, Alabama 35233.
Tel: 205- 934-6762. Fax: 205-934-3425.
Email: mgortk@uab.edu.

Abstract

Retinal ganglion cell (RGC) damage serves as a key indicator of various retinal degenerative diseases, including diabetic retinopathy (DR), glaucoma, retinal arterial and retinal vein occlusions, as well as inflammatory and traumatic optic neuropathies. Despite the growing body of data on the RGC proteomics associated with these conditions, there has been no dedicated study conducted to compare the molecular signaling pathways involved in the mechanism of neuronal cell death. Therefore, we launched the study using two different insults leading to RGC death: glutamate excitotoxicity and optic nerve crush (ONC). C57BL/6 mice were used for the study and underwent NMDA- and ONC-induced damage. Twenty-four hours after ONC and 1 hour after NMDA injection, we collected RGCs using CD90.2 coupled magnetic beads, prepared protein extracts, and employed LC-MS for the global proteomic analysis of RGCs. Statistically significant changes in proteins were analyzed to identify changes to cellular signaling resulting from the treatment. We identified unique and common alterations in protein profiles in RGCs undergoing different types of cellular stresses. Our study not only identified both unique and shared proteomic changes but also laid the groundwork for the future development of a therapeutic platform for testing gene candidates for DR and glaucoma.

Keywords

Retina, Proteomics, Glaucoma, Excitotoxicity, Optic Neuropathy, Ophthalmology

1. Introduction

Retinal ganglion cells (RGCs) are neurons that play a crucial role in vision by transmitting visual information from the retina to the brain. There are several types of RGCs, each with a specific function in processing visual information. They receive input from photoreceptor cells, rods and cones, and integrate this information before sending it to the brain via the optic nerve. The axons of RGCs form the optic nerve, which carries visual signals to the brain, where signals are further processed to create visual perception. Once damaged, axons of the mammalian central nervous system (CNS) fail to regenerate. RGCs are of clinical relevance in diabetic retinopathy (Abu-El-Asrar et al., 2004), glaucoma (Joo et al., 1999), retinal arterial and retinal vein occlusions (Sucher et al., 1997) as well as optic neuropathies (Khan et al., 2021). In these diseases, RGCs may be irreversibly damaged. It is widely accepted that damaged RGCs not only serve as a model of optic neuropathies but also as the primary model for studying mechanisms of CNS axon degeneration and how therapies may promote regeneration.

After insult, both intrinsic and extrinsic factors contribute to whether CNS neurons survive, retain, or regenerate their axons. Although lowering intraocular pressure (IOP) is an approved treatment for glaucoma, it is not effective for every patient, and many other diseases affecting CNS neurons lack approved treatment options. In glaucoma, it has been reported that RGCs undergo apoptosis triggered by various factors, including autophagy, glutamate neurotoxicity, oxidative stress, neuroinflammation, immunity, and vasoconstriction (Kuehn et al., 2005; Shen et al., 2023). Autophagy can be induced by retinal hypoxia and axonal damage (Shen et al., 2023) while glutamate neurotoxicity is induced by the overstimulation of N-methyl-D-aspartate (NMDA) membrane receptors by glutamate, leading to progressive glaucomatous optic neuropathy (Shen et al., 2023).

In diabetes, retinal neuropathy involves progressive RGC death, axonal degeneration, and consequently, optic nerve degeneration (Bikbova et al., 2014). RGC loss occurs in diabetic patients even before the diagnosis of diabetic retinopathy. Furthermore, thinning of both the nerve fiber and the RGC layer has been documented in patients with diabetic retinopathy (Verbraak, 2014; Verma et al., 2009; Vujosevic and Midena, 2013) and animal diabetic models (Oleg S. Gorbatyuk, 2021; Pitale et al., 2021). One of the earliest experimental observations in animal models of diabetic retinopathy (DR) was the impairment of retrograde axonal transport in RGCs (Potilinski et al., 2020). Interestingly, this impairment was found to be even greater in type 1 diabetes than in type 2 diabetes, possibly due to a magnitude of metabolic dysfunctions contributing to optic nerve atrophy (Zhang et al., 1998). Under high glucose conditions, there was an observed increase in glutamate release, leading to significant extracellular glutamate accumulation and subsequent neurotoxicity of RGCs, further contributing to their deterioration (Ma et al., 2010).

Various approaches have been employed to analyze cellular signaling involved in RGC death and axonal deterioration. For instance, research groups have conducted unbiased proteomic screens of total mouse retina lysates (Hollander et al., 2012; Kwong et al., 2021; Magharious et al., 2011; Zhu et al., 2022) and used fluorescent-assisted cell sorting (FACS)(Belin et al., 2015) to isolate RGCs following optic nerve crush (ONC), one of the most extensively studied models of CNS axonal injury. However, these studies either examined whole retina lysates or assessed sorted RGCs at a time point (3 days after injury) when a significant amount of RGC apoptosis has already begun (Goldenberg-Cohen et al., 2012). Another common injury model is NMDA-induced excitotoxicity, a model mimicking the glutamate-induced excitotoxicity associated with multiple neurodegenerative diseases such as amyotrophic lateral sclerosis (ALS), ischemic stroke, and traumatic brain injury. To date, the only study examining proteomics in the context of NMDA-induced excitotoxicity of RGCs investigated proteomic changes in whole retinal lysates 12 hours after NMDA injection, which is a time point at which a substantial amount of RGC apoptosis is already in progress (Suo et al., 2022).

Understanding how CNS neurons respond to injury is crucial as we strive to develop therapeutic strategies for promoting neuroprotection, axon survival, and regeneration. Particularly, the significance of such studies lies in the development of neuroprotective interventions. Therefore, we initiated a comparative proteomic study, in which we analyzed the protein profiles of RGCs subjected to different cellular stress stimuli. The importance of our study lies in the fact that we not only identified differentially expressed proteins involved in two distinct cell death mechanisms but also revealed common biological processes that were similarly altered by different cell stress stimuli.

2. Results

2.1. Nontargeted quantitative proteomics of retinal ganglion cells.

In our study, we adopted an approach to analyze molecular alterations in deteriorating RGCs before rampant cell death ensues, even though the peaks of apoptosis occur at different time points. To investigate early proteomic changes in RGCs following ONC- or NMDA-induced injury, protein lysates from Thy1-magnetic bead-isolated RGCs underwent nano high-performance liquid chromatography/mass spectrometry (LC/MS). RGC enrichment was confirmed via western blot (WB) using antibodies against RGC proteins, RNA-binding protein with multiple splicing (Rbpms), Class III β-tubulin (Tubb3/TUJ1), and photoreceptor markers, phosphodiesterase 6β (Pde6β) and rhodopsin (Rho) (**Fig. 1A**). As expected, RGC markers Rbpms and Tubb3/TUJ1 were highly enriched in RGCs and notably reduced in cells not bound by Cd90.2-coupled magnetic beads, corresponding to the rest of the retinal cells (**Fig. 1A**). Furthermore, photoreceptor proteins Pde6β and rhodopsin were present in trace amounts only in cells bound by the beads but highly expressed in unbound retinal cells. RGC

enrichment was further validated by quantitative reverse transcriptase polymerase chain reaction (qRT-PCR) with primers against CD90/Thy1, Rho, and Pde6b (**Fig. 1B**). While *Thy1* was significantly elevated in cells bound by the magnetic beads and reduced in unbound cells, *Rho* and *Pde6b* mRNA levels were high in unbound cells and significantly diminished in bound cells. Together, the WB and qRT-PCR results indicate reliable RGC enrichment was achieved in our study.

We analyzed identified proteins and prior to pathway analysis, grouped them according to the following parameters: 1) elevated in NMDA treated 2) reduced in NMDA treated 3) elevated in ONC treated 4) reduced in ONC 5) altered in NMDA and ONC.

2.2. NMDA treatment shifts RGC metabolic signaling.

To induce excitotoxic damage to the retina, we intravitreally injected 1 µl of 20 mM NMDA in PBS, following a protocol previously described (Guo et al., 2021). RGCs were isolated 1 hour after NMDA injection and subjected to LC/MS analysis. Levels of many proteins were significantly altered following NMDA injection (see **Figure 2** and **Table 1** for top hits).

Proteins most significantly elevated following NMDA injection include NADH dehydrogenase [ubiquinone] 1 alpha subcomplex subunit 12, 40S ribosomal protein S10, Peptidyl-prolyl cis-trans isomerase FKBP1A, Selenium-binding protein 1, SUMO-activating enzyme subunit 1, Peptidyl-prolyl cis-trans isomerase FKBP4, Probable ATP-dependent RNA helicase DDX28, Translationally-controlled tumor protein, Metastasis-associated protein MTA2, 60S ribosomal protein L35a, and Proteasome subunit alpha type-7, among others. Proteins with the most significant reductions 1 hour after NMDA exposure include Neuronal membrane glycoprotein M6-a, Pyridoxal kinase, AP-2 complex subunit beta, Cytochrome b-c1 complex subunit Rieske-mitochondrial, Catenin beta-1, Cytochrome c-somatic, V-type proton ATPase 116 kDa subunit a isoform 1, Phosphatidate cytidylyltransferase 2, Importin subunit beta-1, Catenin (Cadherin associated protein)-alpha 1, and Mannose-P-dolichol utilization defect 1 protein (**Table 1)**.

The LC/MS results were then subjected to pathway analysis. NMDA treatment resulted in significant alterations in multiple pathways, with a notable impact on metabolic processes (**Table 2**). Pathways most reduced by NMDA injection were neutrophil degranulation, MHC class II antigen presentation, Sertoli cell junction signaling, oxidative phosphorylation, electron transport, TCA Cycle II, signaling by Retinoic Acid, COPI-mediated anterograde transport, and L1CAM interactions. Alterations in these pathways indicate a widespread shift in signaling in RGCs 1 hour after treatment with NMDA. Of note, many pathways involved in ATP production were reduced by NMDA mediated excitotoxicity. In support of these data, **Figure 3** provides a graphical overview of NMDA mediated mitochondrial dysfunction. Therefore, these findings demonstrate that NMDA treatment has a significant impact on

metabolic signaling pathways in retinal ganglion cells, suggesting a link to impaired oxidative stress, and increased apoptosis.

Pathways that were most elevated by NMDA injection were Macrophage Classical Activation Signaling Pathway, Eukaryotic Translation Initiation, Processing of Capped Intron-Containing Pre-mRNA, Eukaryotic Translation Elongation, Major pathway of rRNA processing in the nucleolus and cytosol, Nonsense-Mediated Decay (NMD), Selenoamino acid metabolism, Response of EIF2AK4 (GCN2) to amino acid deficiency, and Eukaryotic Translation Termination **(Table 2)**. These results provide evidence about a shift in protein synthesis following excitotoxic injury (**Table 2**). Consistent with these findings, the levels of specific proteins related to these pathways, such as eukaryotic initiation factor (eIF) 4A2, eIF4B, and eukaryotic elongation factor (eEF) 1b2 were significantly elevated (**Table 1**). RNA processing perturbations are indicated by marked changes in multiple proteins including CPSf6, DNAJC8, RBMX. Collectively, our findings indicate that NMDA excitotoxicity in retinal ganglion cells leads to rapid perturbations in metabolic processes and mitochondrial homeostasis. These perturbations are characterized by a reduction in ATP production pathways. This shift reflects the intricate interplay between NMDA-induced damage and cellular metabolic responses, shedding light on the complex mechanisms involved in excitotoxicity-induced cellular alterations.

2.3. ONC results in metabolic dysfunction

C57BL/6 mice were subjected to ONC as described in a previously published protocol (Guo et al., 2021). RGCs were isolated 24 hours after ONC then subjected to LC/MS analysis. ONC led to alterations in several proteins and pathways (**Figure 4**, **Table 3**, and **Table 4**). The most elevated proteins were Splicing factor 3A subunit 1, CST complex subunit STN1, Stomatin-like protein 2-mitochondrial, DnaJ homolog subfamily C member 8, Arginine and glutamate-rich protein 1, Hepatoma-derived growth factor-related protein 2, Serine/arginine-rich splicing factor 6, Ddx3x protein, Probable ATP-dependent RNA helicase DDX28, RNA-binding protein FUS, and Proteasome subunit beta type-2 (Refer to Table 3 for complete list of top hits).

Proteins most significantly reduced included Importin subunit beta-1, Cytochrome c-somatic, Dihydrolipoyl dehydrogenase-mitochondrial, Protein disulfide-isomerase A4, AP-2 complex subunit beta, Vesicle-associated membrane protein-associated protein A, V-type proton ATPase 116 kDa subunit a isoform 1, Glutathione S-transferase Mu 1, Catenin beta-1, and UMP-CMP kinase, to name a few (**Table 3**). Of note, ONC resulted in perturbations in metabolic signaling cascades. For example, electron transport, oxidative phosphorylation and citric acid cycle signaling were all reduced 24 hours after ONC while Macrophage Classical Activation Signaling pathway was elevated. Overall, the difference in the reduced cellular pathways in RGC with NDMA and ONC demonstrated a few similarities.

For example, the pathways most significantly reduced by ONC induced excitotoxicity were Neutrophil Degranulation, Electron transport, Eicosanoid Signaling, Neutrophil extracellular trap signaling, Oxidative phosphorylation, RHOA signaling, TCA Cycle II, The citric acid cycle and respiratory electron transport, signaling by VEGF, and RAC signaling, among others (**Table 4**).
Signaling most elevated following ONC injury was mitochondrial dysfunction, sirtuin signaling, Processing of Capped Intron-Containing Pre-mRNA, Granzyme A Signaling, Glutaminergic Receptor Signaling Pathway (Enhanced), Autism Signaling Pathway, Docosahexaenoic Acid (DHA) Signaling, Thrombin Signaling, and Integrin Signaling (**Table 4**). **Figure 5** shows the graphical summary of altered signaling pathways in the retina with ONC. As we can see, the major changes in RGC with ONL occurs in cytoskeletal organization.

2.4. ONC and NMDA induced excitotoxicity both alter a subset of proteins

One of the primary objectives of this study was to identify proteins that exhibit changes in multiple models of neuronal injury. In pursuit of this goal, we successfully identified proteins that exhibited alterations in both models (**Fig. 6** and **Table 5**). Remarkably, the majority of these protein level changes, whether upregulation or downregulation, were notably consistent across both groups. Specifically, the most significantly downregulated proteins in both groups were importin subunit beta-1, Cycs, dihydrolipoyl dehydrogenase, protein disfulfide-isomerase a4 (Pdia4), AP-2 complex subunit beta, V-type proton ATPase 116 kDa subunit a isoform 1, Catenin beta-1, Sodium- and chloride-dependent GABA transporter 3, Septin-7, N(G),N(G)-dimethylarginine dimethylaminohydrolase 1, Catenin (Cadherin associated protein)-alpha 1, Microtubule-associated protein 6, and CDGSH iron-sulfur domain-containing protein 1. The most significantly downregulated proteins were alongside significant downregulation of DnaJ homolog subfamily C member 8 (Dnajc8), Probable ATP-dependent RNA helicase DDX28, High mobility group protein B3 (Hmgb3), DNA-(apurinic or apyrimidinic site) endonuclease (Apex1), and Translationally-controlled tumor protein (Tpt1) in both treated RGCs when compared to the control group. To validate the LC/MS proteomics, we assessed levels of Cytochrome C somatic (Cycs), a protein reduced in both ONC and NMDA groups, by western blot (Figure 6B and C). As expected, we also observed a significant reduction in Cycs by western blot. **Table 5**, which provides a visual representation of these modified protein levels, highlights the proteins significantly altered following injury. Two proteins exhibited an opposite trend in the two models. Both Cold-inducible RNA-binding protein and High mobility group protein HMG-I/HMG-Y were upregulated in NMDA challenged RGCs but downregulated following ONC.

The analysis of differentially expressed proteins revealed 28 proteins with significantly reduced expression, 5 proteins with significantly increased expression, and two proteins exhibiting an opposite response pattern to the stimulus in both types of treated RGCs.

3. Discussion

In the present study, we examined acute changes in RGC global protein expression following NMDA injection or ONC. We provide evidence that NMDA excitotoxicity and ONC alters multiple signaling pathways, many of which are metabolic. We identified common proteins and pathways manifesting a decline and elevation in expression.

NMDA excitotoxicity is a model glutamate excitotoxicity. Glutamate excitotoxicity, along with glutamate dysregulation, the primary means by which RGCs are theorized to die in glaucoma and other retinal diseases including diabetic retinopathy (DR). For example, impairment of retrograde axonal transport and glutamate release have been found in animal models of DR (Potilinski et al., 2020). Classically, the primary cause of glutamate excitotoxicity is ATP depletion and impaired glutamate transport, resulting in a buildup of extracellular glutamate, leading to excitotoxicity by overloading NMDA receptor (NMDAR)-expressing cells with Na^+ and Ca^{2+}. Glutamate excitotoxicity is known to be involved in various diseases, including Alzheimer's (Tannenberg et al., 2004), Parkinson's (Verma et al., 2022), or Huntington's (Girling et al., 2018), and predicted to be involved in choroidal vessel occlusion, glaucoma, and diabetic retinopathy (Lucas and Newhouse, 1957; Massey and Miller, 1987, 1990; Thoreson and Witkovsky, 1999; Yumnamcha et al., 2020). Elevated Ca^{2+} can lead to changes in several Ca^{2+}-sensitive signaling cascades and eventually mitochondrial-mediated apoptosis (Verma et al., 2022). An increase in intracellular Na^+ can lead to cell swelling. NMDA-mediated excitotoxicity leads to synaptic degeneration and dendritic pruning before cell death. By isolating RGCs one hour after NMDA injection, we hoped to see how the RGCs are altered in the time window before full-fledged apoptosis begins. We did indeed observe perturbations in several biological processes after NMDA injection. It is possible that the calcium elevation that occurs during excitotoxicity could be the major driving force behind excitotoxic cell death. Cells respond to this is by sequestering this excess calcium in the endoplasmic reticulum and mitochondria. Mitochondria is the site of oxidative phosphorylation, a process that generates ATP and is regulated by calcium (Glancy et al., 2013). This is consistent with our findings on a reduction of signaling cascades related to ATP production.

The murine optic nerve crush injury model is the most commonly used model of RGC injury that mimics molecular events occurring upon traumatic optic neuropathy, glaucoma, etc. (Tang et al., 2011). Moreover, the prevalence of optic neuropathy in diabetics could increase with diabetes duration (Hua et al., 2019). In this model, the crush injury to the optic nerve leads to retinal ganglion cell apoptosis. Like NMDA-induced excitotoxicity, this model can also be used to study the general processes and mechanisms of neuronal death and survival, which is essential for the development of therapeutic measures. In addition, pharmacological and molecular approaches can be used in this model to identify and test potential therapeutic reagents to treat different types of optic neuropathy. Interventions that

are neuroprotective for RGCs challenged with ONC are usually neuroprotective for other CNS neurons (Le Pichon et al., 2017). In addition, axon regeneration promoting treatments discovered with the ONC model can typically promote axon regeneration in the spinal cord (Bhowmick and Abdul-Muneer, 2021). Following ONC, axonal components briefly travel retrogradely prior to the axons returning to the site of injury, only to fail to pass the crush site. In fact, knocking out an inhibitor of the retrograde injury response of RGCs, dual-leucine zipper kinase (DLK), leads to robust RGC survival (Watkins et al., 2013), indicating that retrograde signaling is crucial for cell death signaling following ONC. Based on this, in the earliest response to ONC, we would anticipate changes in the machinery responsible for transport and localization. As expected, we did identify reductions in GO biological processes pertaining to the localization of organelles cellular proteins and cellular macromolecules. After injuring the axon with ONC, we expected to observe changes in synaptic signaling. These changes are presented by the decline in multiple proteins including Catenin beta-1, Sodium- and chloride-dependent GABA transporter 3, AP180 and Synaptotagmin-1. Together, these changes suggest that, as expected, damaging the axon not only disrupts axonal components but also the cellular localization of various cellular entities.

In both RGC degenerative models, we identified common proteins that responded to cellular insults in a similar manner, as well as proteins that exhibited a unique decline in expression in both challenged RGCs. While our current study has its limitations due to the lack of validation of the 33 proteins similarly altered in both groups (**Table 5**), future investigations should prioritize the validation of the roles of these proteins in RGC survival. In particular, it would be interesting to assess the role of these proteins in RGC survival during the development of diabetic retinopathy or glaucoma. For example, Rab18 deficiency detected in both types of challenged RGCs is the molecular deficit underlying Warburg micro syndrome, characterized by eye, nervous system, and endocrine abnormalities (Handley and Sheridan, 1993). Moreover, a recent study highlighted the involvement of Rab18 in lipid metabolism in human diabetic adipose tissue and demonstrated that Rab-18 contributes to insulin resistance in obese individuals. (Guzman-Ruiz et al., 2020; Pulido et al., 2011) Another example is DnaJC8 protein, the effect of which is closely associated with the aggregation of polyQ-containing proteins in a cellular model of spinocerebellar ataxia type 3 (SCA3).(Ito et al., 2016) The authors have shown that DnaJC8 overexpression significantly reduces polyQ aggregation and apoptosis. Therefore, DnaJC8 should be validated for its neuroprotective role in the survival of RGCs undergoing both cellular stressors.

4. Conclusion

In summary, our study was designed to not only identify both individual and shared proteomic changes in retinal ganglion cells undergoing different stress stimuli just before initiating a pro-apoptotic cell death program but also to lay the groundwork for the future development of a therapeutic platform. Future studies should therefore concentrate on validating common proteome changes associated with RGC deterioration in both cell death models. This approach would enhance our understanding of the underlying mechanisms driving RGC degeneration, potentially uncovering key biomarkers or therapeutic targets crucial for developing effective treatments for conditions such as glaucoma, diabetic retinopathy, and optic neuropathies.

5. Methods

5.1. Animals

All animal procedures were approved by The University of Alabama at Birmingham institutional animal use and care (IACUC) committee and in accordance with the statement for the Use of Animals in Ophthalmic and Vision Research by The Association for Research in Vision and Ophthalmology (ARVO). This study is reported in accordance with ARRIVE guidelines. C57BL/6J mice were purchased from Jackson Laboratory (Bar Harbor, ME). An equal number of female and male mice were used in this study (10:10). No difference was observed between male and female mice. For all procedures, mice were anesthetized with ketamine (100 mg/kg) and xylazine (10mg/kg).

To induce injury to RGCs, mice were either intravitreally injected with 1µl of 20mM N-Methyl D aspartic acid (NMDA) or underwent optic nerve crush (ONC) surgery as previously described (Guo et al., 2021). Eyes, either right or left, were selected at random to receive experimental treatment, with unselected contralateral eyes used as controls. Briefly, for ONC, fine tweezers (Dumont#5; Fine Science Tools (FST) Item No. 11254-20 or Dumont#55; FST Item No. 11255-20) were used to create a small incision in the conjunctiva and then maneuvered between extraocular muscles to access the optic nerve, which was gently squeezed for 5 seconds at a location approximately 1mm posterior to the globe using Dumont #5 tweezers.

5.2. RGC Isolation

To isolate RGCs, we used a method that has previously been verified with slight modifications. To ensure enough tissue for proteomics, 5 retinas were pooled per experimental unit to create n=4 per group. Briefly, animals from each group were euthanized with CO_2 asphyxiation and their retinas were harvested in cold neurobasal medium and placed in a 37°C water bath for 5 minutes. The neurobasal media was removed and replaced with fresh pre-warmed neurobasal media containing papain (0.06mg/ml or 33.4 U/mg) and 5mM L-cysteine and incubated 20 minutes at 37°C. The papain solution

was removed and replaced with neurobasal containing 2mM L-Glutamine (Gibco; Catalog no. 25030081) B-27 supplement (Gibco; Catalog no. 17504044) and 10% FBS (Gibco; Catalog no. 26140079). The retinas were dissociated by gently pipetting up and down with a wide bore 1ml pipette tip. Cells were then centrifuged at 450g for 8 minutes and resuspended in 90 µl of isolation buffer (DPBS + 0.5% BSA + 2mM EDTA) containing 25 µg/ml DNAse I + 5mM MgCl2. Cells were filtered through a 30µm cell strainer and incubated with CD90.2 magnetic beads (Miltenyi Biotec; Catalog no. 130-121-278) at 4°C for 10 minutes and then isolated using MACs LS (Miltenyi Biotec; Catalog no. 130-042-401) columns following the manufacturer's instructions. After isolation, cells were washed with DPBS, centrifuged at 450g for 8 minutes and their pellets stored at -70°C prior to proteomics sample preparation and LC/MS analysis.

5.3. Western Blotting

Enriched RGCs were lysed in RIPA buffer (Cell Signaling Technology, Cat: 9806) and protein concentrations were determined by Bio-Rad protein assay reagent (Cat: 5000006). Ten micrograms of protein were separated by SDS-PAGE and transferred to a PVDF membrane. After blocking with milk, membranes were then incubated with primary antibodies (1:2000 dilution) of interest (Rbpms-MilliporeSigma, Cat:ABN1362, Lot:3782213. TUJ1/TUBB3-Biolegend, Cat:801203, Lot:B373939. PDE6β-invitrogen, Cat:PA1-722, Lot: YA369623,; Rhodopsin- University of British Columbia, Rho 1D4, Lot: 1019 . β-actin-MilliporeSigma, Cat: A2228, Lot:118M4829V), followed by HRP-conjugated secondary antibodies (Li-COR; Anti-mouse Cat: 926-80010, Lot:D20526-01 Anti-rabbit Cat: 926-80011, Lot: D10601-03) and lastly imaged on a Li-COR Odyssey Imaging System.

5.4. qRT-PCR

RNA was isolated from enriched RGCs using an RNeasy Micro Kit (Qiagen, 74004). RNA content was measured with a nanodrop spectrophotometer. cDNA was prepared using Bio-Rad iScript cDNA Synthesis Kit (1708891) following the manufacturer's instructions. qRT-PCR was carried out on an Applied Biosystems QuantStudio 3. Predesigned primers were purchased from ThermoFisher (Gapdh-Mm99999915_g1, Rhodopsin- Mm01184405_m1 and Thy1- Mm00493681_m1).

5.5. Proteomics

5.5.1. LC/MS

Proteomics analysis was carried out as previously described with minor changes (Ludwig et al., 2016), within section 2.5 nLC-ESI-MS2 under Protein IDs for GeLC. Proteins from isolated RGCs were extracted using T-PER™ Mammalian Protein Extraction Reagent (Thermo Fisher Scientific, Cat.# 78510) supplemented with HALT protease inhibitor cocktail (Thermo Fisher Scientific, Cat.# 78425),

and benzonase nuclease (Sigma, E1014) following manufacturers instructions. Lysates were quantified using Pierce BCA Protein Assay Kit (Thermo Fisher Scientific, Cat.# 23227). Samples were prepared in NuPAGE LDS sample buffer (1x final conc., Invitrogen, Cat.# NP0007) and reduced with DTT then denatured at 70°C for 10min prior to loading 20µg onto Novex NuPAGE 10% Bis-Tris Protein gels (Invitrogen, Cat.# NP0315BOX) and separated appropriately (@ 200 constant V). The gels were stained overnight with Novex Colloidal Blue Staining kit (Invitrogen, Cat.# LC6025). Following de-staining, each entire lane was cut into multiple MW and equilibrated in 100 mM ammonium bicarbonate (AmBc), each gel plug was then digested overnight with Trypsin Gold, Mass Spectrometry Grade (Promega, Cat.# V5280) following manufacturer's instruction. Peptide extracts were reconstituted in 0.1% Formic Acid/ddH2O at 0.1µg/µL.

Peptide digests (8µL each) were injected onto a 1260 Infinity nHPLC stack (Agilent Technologies), and separated using a 75 micron I.D. x 15 cm pulled tip C-18 column (Jupiter C-18 300 Å, 5 micron, Phenomenex). This system runs in-line with a Thermo Q Exactive HFx mass spectrometer, equipped with a Nanospray Flex™ ion source (Thermo Fisher Scientific), and all data were collected in CID mode. The nHPLC is configured with binary mobile phases that includes solvent A (0.1%FA in ddH2O), and solvent B (0.1%FA in 15% ddH2O/85% ACN), programmed as follows; 10min @ 5%B (2µL/min, load), 30min @ 5%-40%B (linear: 0.5nL/min, analyze), 5min @ 70%B (2µL/min, wash), 10min @ 0%B (2µL/min, equilibrate). Following each parent ion scan (300-1200m/z @ 60k resolution), fragmentation data (MS2) were collected on the top most intense 18 ions @7.5K resolution. For data dependent scans, charge state screening and dynamic exclusion were enabled with a repeat count of 2, repeat duration of 30s, and exclusion duration of 90s.

MS data conversion and searches The XCalibur RAW files were collected in profile mode, centroided and converted to MzXML using ReAdW v. 3.5.1. The mgf files were created using MzXML2Search (included in TPP v. 3.5) for all scans. The data was searched using SEQUEST (Thermo Fisher Scientific), which is set for three maximum missed cleavages, a precursor mass window of 20ppm, trypsin digestion, variable modification C @ 57.0293, and M @ 15.9949 as a base setting. Searches were performed with the mus musculus species specific subset of the UniProtKB database.

5.5.2. Peptide filtering, grouping, and quantification

The list of peptide IDs generated based on SEQUEST search results were filtered using Scaffold (Protein Sciences, Portland Oregon). Scaffold filters and groups all peptides to generate and retain only high confidence IDs while also generating normalized spectral counts (N-SC's) across all samples for the purpose of relative quantification. The filter cut-off values were set with minimum peptide length of >5 AA's, with no MH+1 charge states, with peptide probabilities of >80% C.I., and with the number of peptides per protein ≥2. The protein probabilities will be set to a >99.0% C.I., and an FDR<1.0. Scaffold

incorporates the two most common methods for statistical validation of large proteome datasets, the false discovery rate (FDR) and protein probability (Keller, Nesvizhskii, Weatherly). Relative quantification across experiments were then performed via spectral counting (Old, Liu), and when relevant, spectral count abundances will then be normalized between samples (Hyde).

5.5.3. Statistical analysis

For generated proteomic data, two separate non-parametric-like statistical analyses were performed between each pair-wise comparison. These analyses included; A) the calculation of weight values by significance analysis of microarray (SAM; cut off >|0.8| combined with, B) T-Test (single tail, unequal variance, cut off of $p < 0.05$), which are then sorted according to the highest statistical relevance in each comparison. For SAM, the weight value (W) is a function statistically derived that approaches significance as the distance between the means ($\mu1-\mu2$) for each group increases, and the SD ($\delta1-\delta2$) decreases using the formula: $W=(\mu1-\mu2)/(\delta1-\delta2)$. For protein abundance ratios determined with N-SC's, we set a 1.5-fold change as the threshold for significance, determined empirically by analyzing the inner-quartile data from the control experiments using ln-ln plots, where the Pierson's correlation coefficient (R) is 0.98, and >99% of the normalized intensities fell between the set fold change. Each of the tests (SAM, Ttest, and fold change) must be passed for to be considered significant.

Funding

This work was supported by the National Eye Institute, grants R01 EY027763.

Author contributions

MG and CS designed the study. CS performed animal work. JM perfomed the proteomic study. MG, JM, and CS analyzed the data. MG and CS wrote the manuscript and prepared the figures.

Competing interests

The author(s) declare no competing interests.

Figure Legends

Figure 1. RGCs are enriched with Cd90.2 coupled magnetic beads. A) Western blot of select RGC and photoreceptor proteins indicating RGC enrichment. B) qRT-PCR analysis using primers against RGC or photoreceptor targets. * = $p<0.05$, *** = $p<0.005$, **** = $p<0.001$ (n=3-4). Data are shown as a standard deviation.

Figure 2. Proteins changed in RGCs 1 hour after following NMDA induced excitotoxicity. Heatmap depicting levels of protein top-hits.

Figure 3. NMDA induced excitotoxicity induces alterations in metabolic signaling. Summary graph highlighting changes in mitochondrial signaling.

Figure 4. ONC results in changes in levels of proteins. Heatmap showing levels of proteins most changed 24 hours after ONC.

Figure 5. ONC leads to changes in cellular organization. Graphical summary detailing changes in cellular organization following ONC.

Figure 6. Proteins changed in RGCs 1 hour after NMDA induced excitoxicity as well as 24 hours after ONC. A) Heatmap identifying top-hits. B) Western Blots of protein lysates from enriched RGCs. C) Graph depicting Cycs levels normalized to β-actin. A.U. = arbitrary units. **=p<0.01

Table Legends

Table 1. List of proteins most differentially expressed in RGCs 1 hour after NMDA treatment.

Table 2. Ingenuity pathways significantly changed by NMDA-induced excitotoxicity.

Table 3. List of proteins with the largest fold-changes in RGCs 24 hours after ONC.

Table 4. List of ingenuity pathways significantly altered in RGCs 24 hours after ONC.

Table 5. Proteins significantly changed in RGCs in both treatment groups, NMDA and ONC.

References

Abu-El-Asrar, A.M., Dralands, L., Missotten, L., Al-Jadaan, I.A., Geboes, K., 2004. Expression of apoptosis markers in the retinas of human subjects with diabetes. Invest Ophthalmol Vis Sci 45, 2760-2766.

Belin, S., Nawabi, H., Wang, C., Tang, S., Latremoliere, A., Warren, P., Schorle, H., Uncu, C., Woolf, C.J., He, Z., Steen, J.A., 2015. Injury-Induced Decline of Intrinsic Regenerative Ability Revealed by Quantitative Proteomics. Neuron 86, 1000-1014.

Bhowmick, S., Abdul-Muneer, P.M., 2021. PTEN Blocking Stimulates Corticospinal and Raphespinal Axonal Regeneration and Promotes Functional Recovery After Spinal Cord Injury. J Neuropathol Exp Neurol 80, 169-181.

Bikbova, G., Oshitari, T., Baba, T., Yamamoto, S., 2014. Neurotrophic factors for retinal ganglion cell neuropathy - with a special reference to diabetic neuropathy in the retina. Curr Diabetes Rev 10, 166-176.

Girling, K.D., Demers, M.J., Laine, J., Zhang, S., Wang, Y.T., Graham, R.K., 2018. Activation of caspase-6 and cleavage of caspase-6 substrates is an early event in NMDA receptor-mediated excitotoxicity. J Neurosci Res 96, 391-406.

Glancy, B., Willis, W.T., Chess, D.J., Balaban, R.S., 2013. Effect of calcium on the oxidative phosphorylation cascade in skeletal muscle mitochondria. Biochemistry 52, 2793-2809.

Goldenberg-Cohen, N., Raiter, A., Gaydar, V., Dratviman-Storobinsky, O., Goldstein, T., Weizman, A., Hardy, B., 2012. Peptide-binding GRP78 protects neurons from hypoxia-induced apoptosis. Apoptosis 17, 278-288.

Guo, X., Starr, C., Zhou, J., Chen, B., 2021. Protocol for evaluating the role of a gene in protecting mouse retinal ganglion cells. STAR Protoc 2, 100932.

Guzman-Ruiz, R., Tercero-Alcazar, C., Rabanal-Ruiz, Y., Diaz-Ruiz, A., El Bekay, R., Rangel-Zuniga, O.A., Navarro-Ruiz, M.C., Molero, L., Membrives, A., Ruiz-Rabelo, J.F., Pandit, A., Lopez-Miranda, J., Tinahones, F.J., Malagon, M.M., 2020. Adipose tissue depot-specific intracellular and extracellular cues contributing to insulin resistance in obese individuals. FASEB J 34, 7520-7539.

Handley, M., Sheridan, E., 1993. RAB18 Deficiency, in: Adam, M.P., Mirzaa, G.M., Pagon, R.A., Wallace, S.E., Bean, L.J.H., Gripp, K.W., Amemiya, A. (Eds.), GeneReviews((R)), Seattle (WA).

Hollander, A., D'Onofrio, P.M., Magharious, M.M., Lysko, M.D., Koeberle, P.D., 2012. Quantitative retinal protein analysis after optic nerve transection reveals a neuroprotective role for hepatoma-derived growth factor on injured retinal ganglion cells. Invest Ophthalmol Vis Sci 53, 3973-3989.
Hua, R., Qu, L., Ma, B., Yang, P., Sun, H., Liu, L., 2019. Diabetic Optic Neuropathy and Its Risk Factors in Chinese Patients With Diabetic Retinopathy. Invest Ophthalmol Vis Sci 60, 3514-3519.
Ito, N., Kamiguchi, K., Nakanishi, K., Sokolovskya, A., Hirohashi, Y., Tamura, Y., Murai, A., Yamamoto, E., Kanaseki, T., Tsukahara, T., Kochin, V., Chiba, S., Shimohama, S., Sato, N., Torigoe, T., 2016. A novel nuclear DnaJ protein, DNAJC8, can suppress the formation of spinocerebellar ataxia 3 polyglutamine aggregation in a J-domain independent manner. Biochem Biophys Res Commun 474, 626-633.
Joo, C.K., Choi, J.S., Ko, H.W., Park, K.Y., Sohn, S., Chun, M.H., Oh, Y.J., Gwag, B.J., 1999. Necrosis and apoptosis after retinal ischemia: involvement of NMDA-mediated excitotoxicity and p53. Invest Ophthalmol Vis Sci 40, 713-720.
Khan, R.S., Ross, A.G., Aravand, P., Dine, K., Selzer, E.B., Shindler, K.S., 2021. RGC and Vision Loss From Traumatic Optic Neuropathy Induced by Repetitive Closed Head Trauma Is Dependent on Timing and Force of Impact. Transl Vis Sci Technol 10, 8.
Kuehn, M.H., Fingert, J.H., Kwon, Y.H., 2005. Retinal ganglion cell death in glaucoma: mechanisms and neuroprotective strategies. Ophthalmol Clin North Am 18, 383-395, vi.
Kwong, J.M.K., Caprioli, J., Sze, Y.H., Yu, F.J., Li, K.K., To, C.H., Lam, T.C., 2021. Differential Retinal Protein Expression in Primary and Secondary Retinal Ganglion Cell Degeneration Identified by Integrated SWATH and Target-Based Proteomics. Int J Mol Sci 22.
Le Pichon, C.E., Meilandt, W.J., Dominguez, S., Solanoy, H., Lin, H., Ngu, H., Gogineni, A., Sengupta Ghosh, A., Jiang, Z., Lee, S.-H., Maloney, J., Gandham, V.D., Pozniak, C.D., Wang, B., Lee, S., Siu, M., Patel, S., Modrusan, Z., Liu, X., Rudhard, Y., Baca, M., Gustafson, A., Kaminker, J., Carano, R.A.D., Huang, E.J., Foreman, O., Weimer, R., Scearce-Levie, K., Lewcock, J.W., 2017. Loss of dual leucine zipper kinase signaling is protective in animal models of neurodegenerative disease. Science Translational Medicine 9, eaag0394.
Lucas, D.R., Newhouse, J.P., 1957. The toxic effect of sodium L-glutamate on the inner layers of the retina. AMA Arch Ophthalmol 58, 193-201.
Ludwig, M.R., Kojima, K., Bowersock, G.J., Chen, D., Jhala, N.C., Buchsbaum, D.J., Grizzle, W.E., Klug, C.A., Mobley, J.A., 2016. Surveying the serologic proteome in a tissue-specific kras(G12D) knockin mouse model of pancreatic cancer. Proteomics 16, 516-531.
Ma, R., Xie, X.J., Wan, L., 2010. [Effect of drug-serum with Chinese drugs for nourishing shen and activating blood on the glutamate release in purified retinal ganglion cells cultured in high-glucose conditions]. Zhongguo Zhong Xi Yi Jie He Za Zhi 30, 875-879.
Magharious, M., D'Onofrio, P.M., Hollander, A., Zhu, P., Chen, J., Koeberle, P.D., 2011. Quantitative iTRAQ analysis of retinal ganglion cell degeneration after optic nerve crush. J Proteome Res 10, 3344-3362.
Massey, S.C., Miller, R.F., 1987. Excitatory amino acid receptors of rod- and cone-driven horizontal cells in the rabbit retina. J Neurophysiol 57, 645-659.
Massey, S.C., Miller, R.F., 1990. N-methyl-D-aspartate receptors of ganglion cells in rabbit retina. J Neurophysiol 63, 16-30.
Oleg S. Gorbatyuk, P.M.P., Irina V. Saltykova, Iuliia B. Dorofeeva, Assylbek A. Zhylkibayev, Mohammad Athar, Preston A. Fuchs, Brian C. Samuels and Marina S. Gorbatyuk, 2021. A Novel Tree Shrew Model of Diabetic Retinopathy. Front Endocrinol (Lausanne).
Pitale, P.M., Saltykova, I.V., Adu-Agyeiwaah, Y., Calzi, S.L., Satoh, T., Akira, S., Gorbatyuk, O., Boulton, M.E., Pardue, M.T., Garvey, W.T., Athar, M., Grant, M.B., Gorbatyuk, M.S., 2021. Tribbles Homolog 3 Mediates the Development and Progression of Diabetic Retinopathy. Diabetes.
Potilinski, M.C., Lorenc, V., Perisset, S., Gallo, J.E., 2020. Mechanisms behind Retinal Ganglion Cell Loss in Diabetes and Therapeutic Approach. Int J Mol Sci 21.
Pulido, M.R., Diaz-Ruiz, A., Jimenez-Gomez, Y., Garcia-Navarro, S., Gracia-Navarro, F., Tinahones, F., Lopez-Miranda, J., Fruhbeck, G., Vazquez-Martinez, R., Malagon, M.M., 2011. Rab18 dynamics in adipocytes in relation to lipogenesis, lipolysis and obesity. PLoS One 6, e22931.
Shen, W.C., Huang, B.Q., Yang, J., 2023. Regulatory mechanisms of retinal ganglion cell death in normal tension glaucoma and potential therapies. Neural Regen Res 18, 87-93.
Sucher, N.J., Lipton, S.A., Dreyer, E.B., 1997. Molecular basis of glutamate toxicity in retinal ganglion cells. Vision Res 37, 3483-3493.

Suo, L., Dai, W., Chen, X., Qin, X., Li, G., Song, S., Zhang, D., Zhang, C., 2022. Proteomics analysis of N-methyl-d-aspartate-induced cell death in retinal and optic nerves. J Proteomics 252, 104427.
Tang, Z., Zhang, S., Lee, C., Kumar, A., Arjunan, P., Li, Y., Zhang, F., Li, X., 2011. An optic nerve crush injury murine model to study retinal ganglion cell survival. J Vis Exp.
Tannenberg, R.K., Scott, H.L., Westphalen, R.I., Dodd, P.R., 2004. The identification and characterization of excitotoxic nerve-endings in Alzheimer disease. Curr Alzheimer Res 1, 11-25.
Thoreson, W.B., Witkovsky, P., 1999. Glutamate receptors and circuits in the vertebrate retina. Prog Retin Eye Res 18, 765-810.
Verbraak, F.D., 2014. Neuroretinal degeneration in relation to vasculopathy in diabetes. Diabetes 63, 3590-3592.
Verma, A., Rani, P.K., Raman, R., Pal, S.S., Laxmi, G., Gupta, M., Sahu, C., Vaitheeswaran, K., Sharma, T., 2009. Is neuronal dysfunction an early sign of diabetic retinopathy? Microperimetry and spectral domain optical coherence tomography (SD-OCT) study in individuals with diabetes, but no diabetic retinopathy. Eye (Lond) 23, 1824-1830.
Verma, M., Lizama, B.N., Chu, C.T., 2022. Excitotoxicity, calcium and mitochondria: a triad in synaptic neurodegeneration. Transl Neurodegener 11, 3.
Vujosevic, S., Midena, E., 2013. Retinal layers changes in human preclinical and early clinical diabetic retinopathy support early retinal neuronal and Muller cells alterations. J Diabetes Res 2013, 905058.
Watkins, T.A., Wang, B., Huntwork-Rodriguez, S., Yang, J., Jiang, Z., Eastham-Anderson, J., Modrusan, Z., Kaminker, J.S., Tessier-Lavigne, M., Lewcock, J.W., 2013. DLK initiates a transcriptional program that couples apoptotic and regenerative responses to axonal injury. Proceedings of the National Academy of Sciences 110, 4039-4044.
Yumnamcha, T., Guerra, M., Singh, L.P., Ibrahim, A.S., 2020. Metabolic Dysregulation and Neurovascular Dysfunction in Diabetic Retinopathy. Antioxidants (Basel) 9.
Zhang, L., Inoue, M., Dong, K., Yamamoto, M., 1998. Alterations in retrograde axonal transport in optic nerve of type I and type II diabetic rats. Kobe J Med Sci 44, 205-215.
Zhu, Y., Zhang, Y., Qi, X., Lian, Y., Che, H., Jia, J., Yang, C., Xu, Y., Chi, X., Jiang, W., Li, Y., Mi, J., Yang, Y., Li, X., Tian, G., 2022. GAD1 alleviates injury-induced optic neurodegeneration by inhibiting retinal ganglion cell apoptosis. Exp Eye Res 223, 109201.

Figure Legends

Figure 1. RGCs are enriched with Cd90.2 coupled magnetic beads. A) Western blot of select RGC and photoreceptor proteins indicating RGC enrichment. B) qRT-PCR analysis using primers against RGC or photoreceptor targets. * = $p<0.05$, *** = $p<0.005$, **** = $p<0.001$ (n=3-4). Data are shown as a standard deviation.

Figure 2. Proteins changed in RGCs 1 hour after following NMDA induced excitotoxicity. Heatmap depicting levels of protein top-hits.

Figure 3. NMDA induced excitotoxicity induces alterations in metabolic signaling. Summary graph highlighting changes in mitochondrial signaling.

Figure 4. ONC results in changes in levels of proteins. Heatmap showing levels of proteins most changed 24 hours after ONC.

Figure 5. ONC leads to changes in cellular organization. Graphical summary detailing changes in cellular organization following ONC.

Figure 6. Proteins changed in RGCs 1 hour after NMDA induced excitoxicity as well as 24 hours after ONC. A) Heatmap identifying top-hits. B) Western Blots of protein lysates from enriched RGCs. C) Graph depicting Cycs levels normalized to β-actin. A.U. = arbitrary units. **=$p<0.01$

Table Legends

Table 1. List of proteins most differentially expressed in RGCs 1 hour after NMDA treatment.

Table 2. Ingenuity pathways significantly changed by NMDA-induced excitotoxicity.

Table 3. List of proteins with the largest fold-changes in RGCs 24 hours after ONC.

Table 4. List of ingenuity pathways significantly altered in RGCs 24 hours after ONC.

Table 5. Proteins significantly changed in RGCs in both treatment groups, NMDA and ONC.

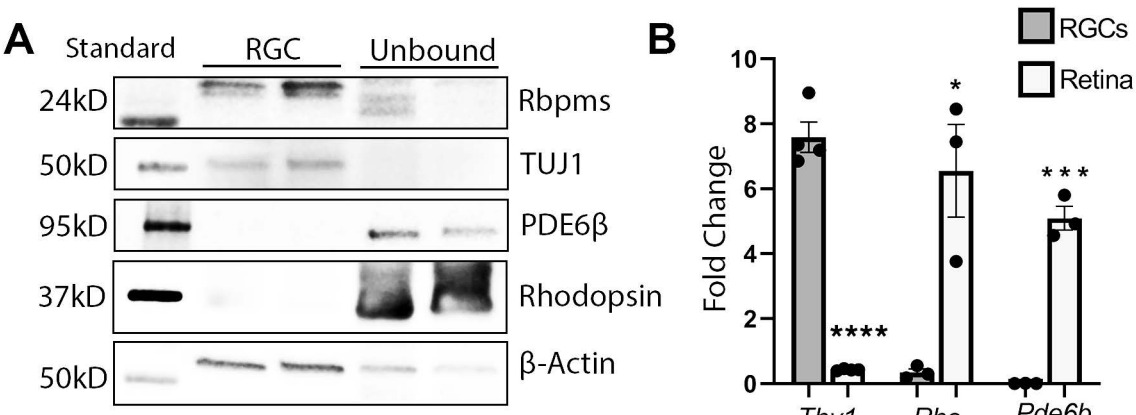
A
Standard
RGC
Unbound
24kD
Rbpms
50kD
TUJ1
95kD
PDE6β
37kD
Rhodopsin
50kD
β-Actin
B
RGCs
Retina
Fold Change
10
8
6
4
2
0
****
*
***
Thy1
Rho
Pde6b

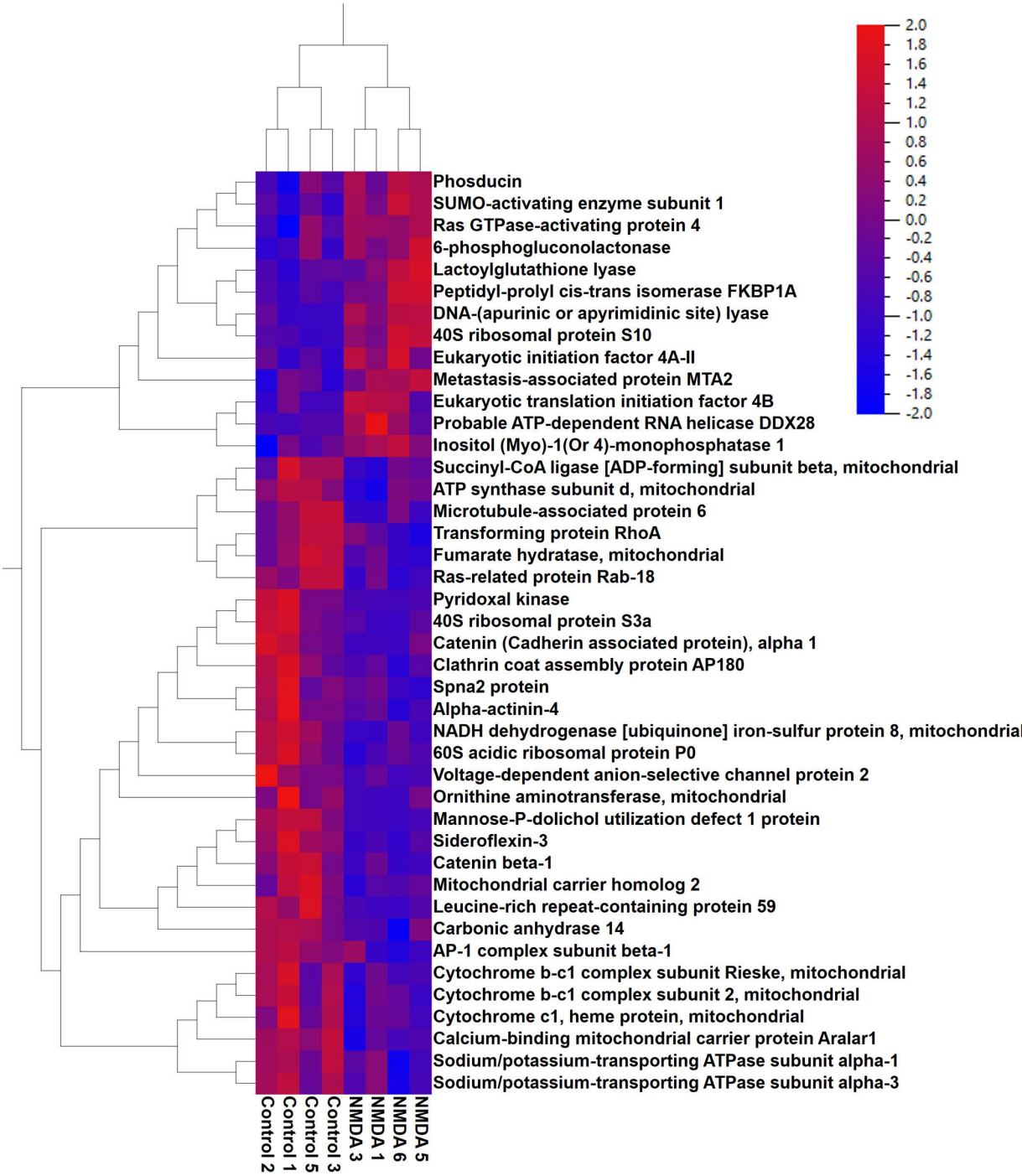
Phosducin
SUMO-activating enzyme subunit 1
Ras GTPase-activating protein 4
6-phosphogluconolactonase
Lactoylglutathione lyase
Peptidyl-prolyl cis-trans isomerase FKBP1A
DNA-(apurinic or apyrimidinic site) lyase
40S ribosomal protein S10
Eukaryotic initiation factor 4A-II
Metastasis-associated protein MTA2
Eukaryotic translation initiation factor 4B
Probable ATP-dependent RNA helicase DDX28
Inositol (Myo)-1(Or 4)-monophosphatase 1
Succinyl-CoA ligase [ADP-forming] subunit beta, mitochondrial
ATP synthase subunit d, mitochondrial
Microtubule-associated protein 6
Transforming protein RhoA
Fumarate hydratase, mitochondrial
Ras-related protein Rab-18
Pyridoxal kinase
40S ribosomal protein S3a
Catenin (Cadherin associated protein), alpha 1
Clathrin coat assembly protein AP180
Spna2 protein
Alpha-actinin-4
NADH dehydrogenase [ubiquinone] iron-sulfur protein 8, mitochondrial
60S acidic ribosomal protein P0
Voltage-dependent anion-selective channel protein 2
Ornithine aminotransferase, mitochondrial
Mannose-P-dolichol utilization defect 1 protein
Sideroflexin-3
Catenin beta-1
Mitochondrial carrier homolog 2
Leucine-rich repeat-containing protein 59
Carbonic anhydrase 14
AP-1 complex subunit beta-1
Cytochrome b-c1 complex subunit Rieske, mitochondrial
Cytochrome b-c1 complex subunit 2, mitochondrial
Cytochrome c1, heme protein, mitochondrial
Calcium-binding mitochondrial carrier protein Aralar1
Sodium/potassium-transporting ATPase subunit alpha-1
Sodium/potassium-transporting ATPase subunit alpha-3
Control 2
Control 1
Control 5
Control 3
NMDA 3
NMDA 1
NMDA 6
NMDA 5
2.0
1.8
1.6
1.4
1.2
1.0
0.8
0.6
0.4
0.2
0.0
-0.2
-0.4
-0.6
-0.8
-1.0
-1.2
-1.4
-1.6
-1.8
-2.0

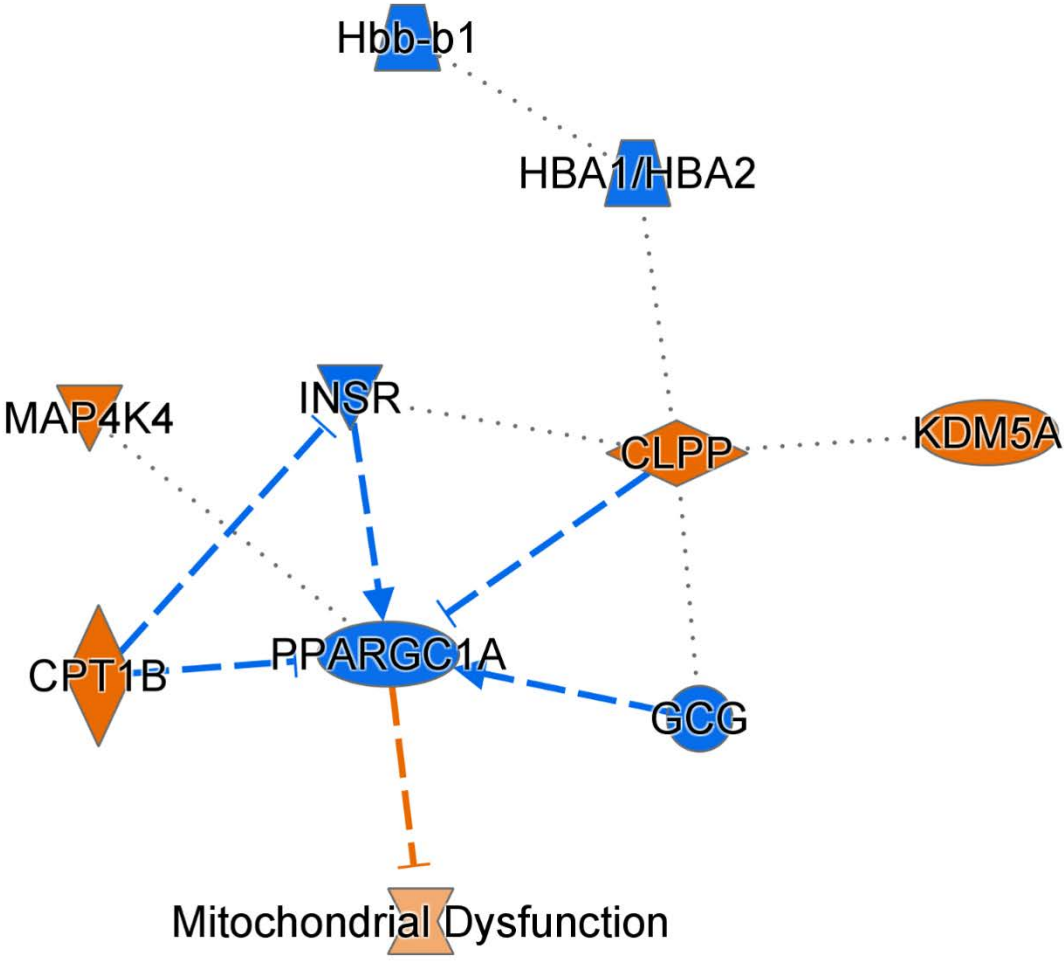
Hbb-b1
HBA1/HBA2
MAP4K4
INSR
CLPP
KDM5A
CPT1B
PPARGC1A
GCG
Mitochondrial Dysfunction

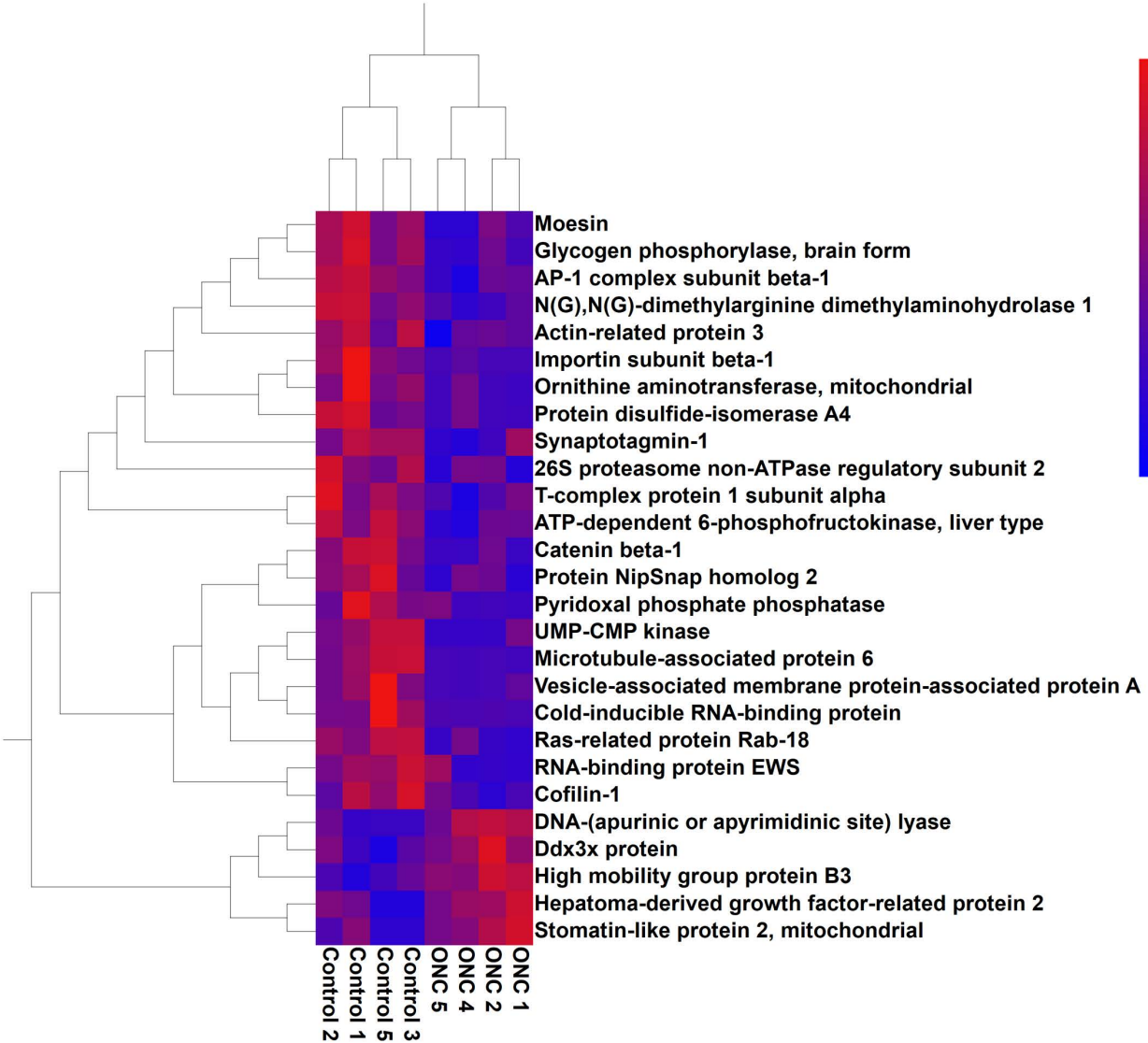
Moesin
Glycogen phosphorylase, brain form
AP-1 complex subunit beta-1
N(G),N(G)-dimethylarginine dimethylaminohydrolase 1
Actin-related protein 3
Importin subunit beta-1
Ornithine aminotransferase, mitochondrial
Protein disulfide-isomerase A4
Synaptotagmin-1
26S proteasome non-ATPase regulatory subunit 2
T-complex protein 1 subunit alpha
ATP-dependent 6-phosphofructokinase, liver type
Catenin beta-1
Protein NipSnap homolog 2
Pyridoxal phosphate phosphatase
UMP-CMP kinase
Microtubule-associated protein 6
Vesicle-associated membrane protein-associated protein A
Cold-inducible RNA-binding protein
Ras-related protein Rab-18
RNA-binding protein EWS
Cofilin-1
DNA-(apurinic or apyrimidinic site) lyase
Ddx3x protein
High mobility group protein B3
Hepatoma-derived growth factor-related protein 2
Stomatin-like protein 2, mitochondrial
Control 2
Control 1
Control 5
Control 3
ONC 5
ONC 4
ONC 2
ONC 1
2.0
1.8
1.6
1.4
1.2
1.0
0.8
0.6
0.4
0.2
0.0
-0.2
-0.4
-0.6
-0.8
-1.0
-1.2
-1.4
-1.6
-1.8
-2.0

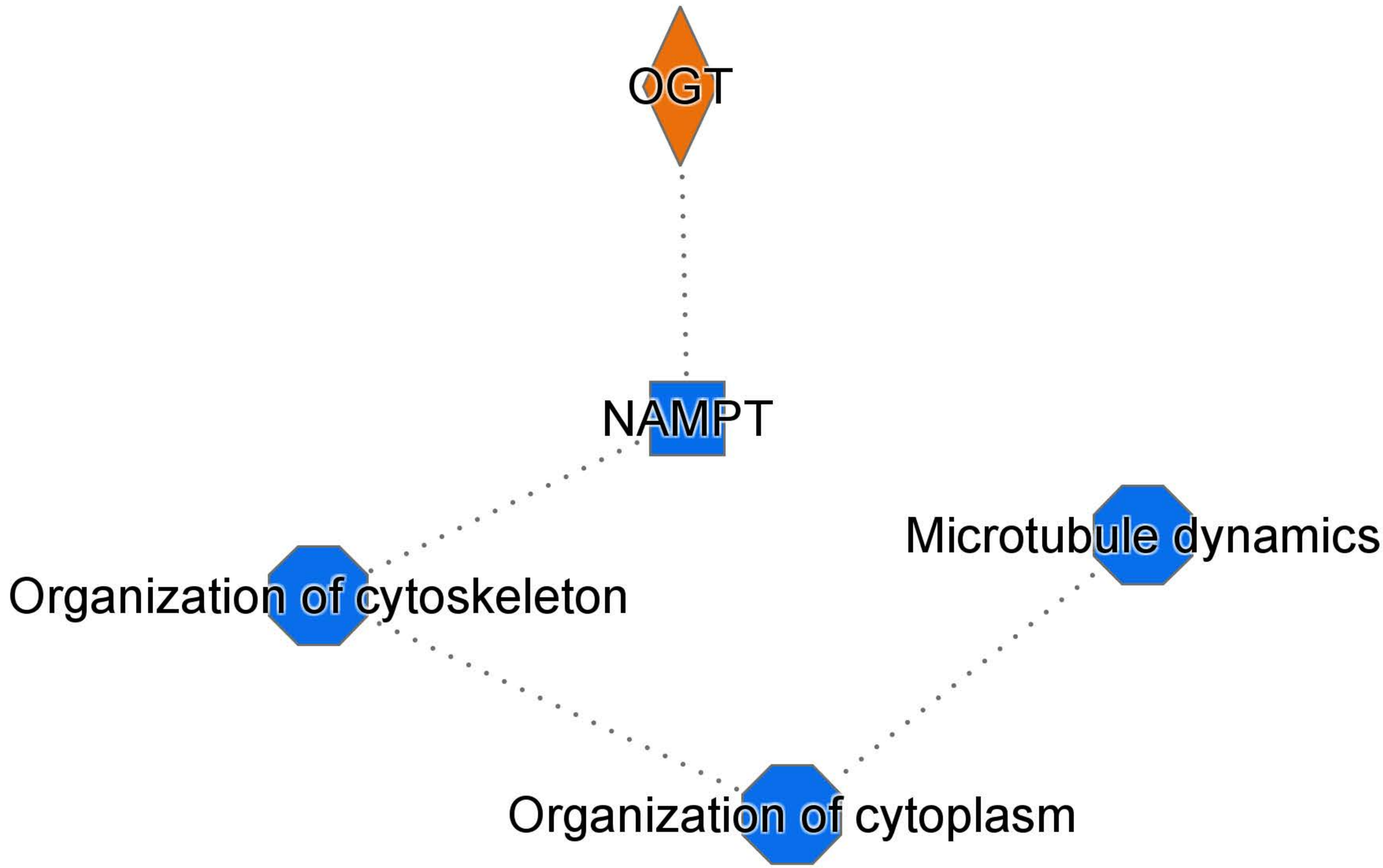
OGT
NAMPT
Microtubule dynamics
Organization of cytoskeleton
Organization of cytoplasm

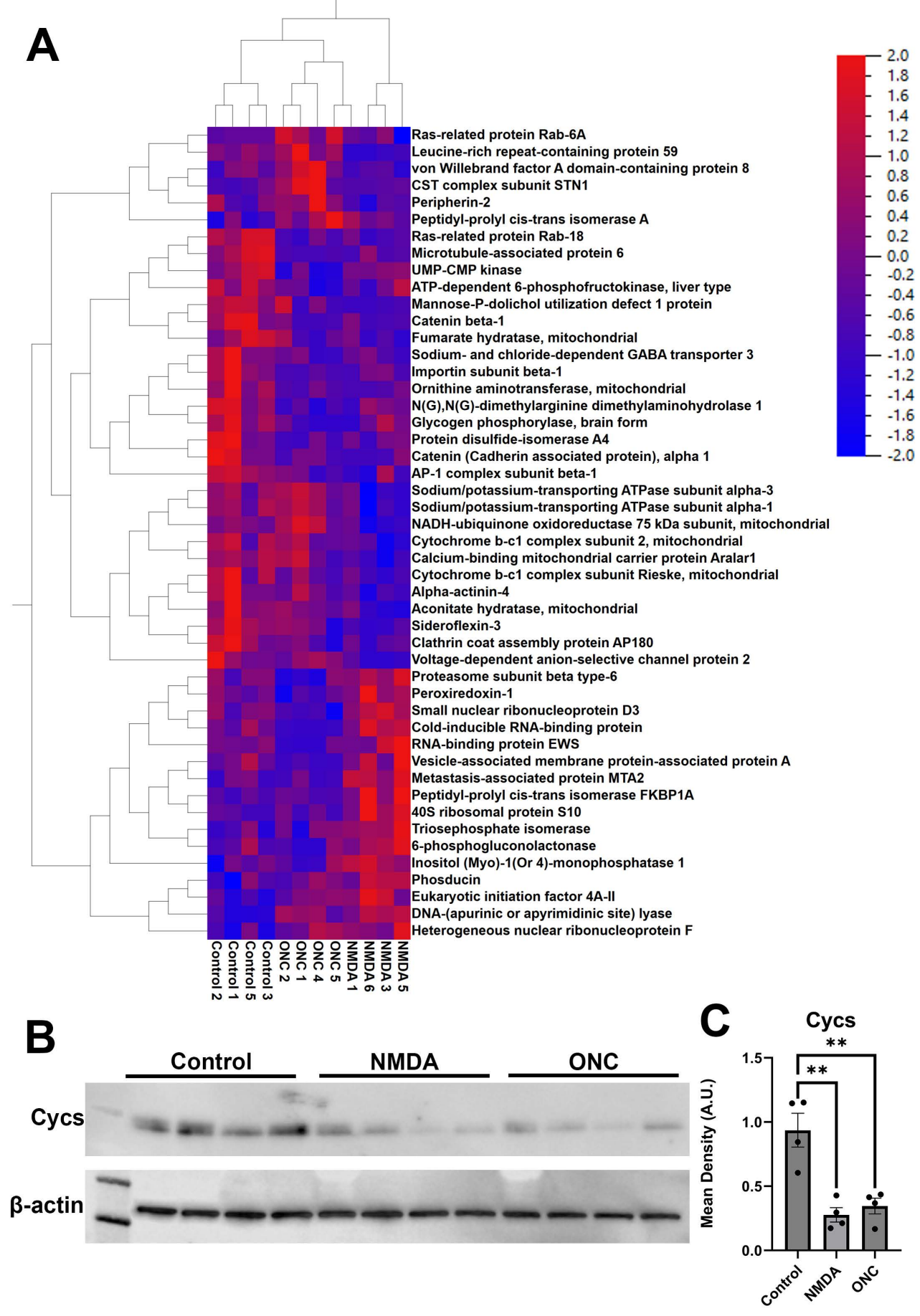
A
Ras-related protein Rab-6A
Leucine-rich repeat-containing protein 59
von Willebrand factor A domain-containing protein 8
CST complex subunit STN1
Peripherin-2
Peptidyl-prolyl cis-trans isomerase A
Ras-related protein Rab-18
Microtubule-associated protein 6
UMP-CMP kinase
ATP-dependent 6-phosphofructokinase, liver type
Mannose-P-dolichol utilization defect 1 protein
Catenin beta-1
Fumarate hydratase, mitochondrial
Sodium- and chloride-dependent GABA transporter 3
Importin subunit beta-1
Ornithine aminotransferase, mitochondrial
N(G),N(G)-dimethylarginine dimethylaminohydrolase 1
Glycogen phosphorylase, brain form
Protein disulfide-isomerase A4
Catenin (Cadherin associated protein), alpha 1
AP-1 complex subunit beta-1
Sodium/potassium-transporting ATPase subunit alpha-3
Sodium/potassium-transporting ATPase subunit alpha-1
NADH-ubiquinone oxidoreductase 75 kDa subunit, mitochondrial
Cytochrome b-c1 complex subunit 2, mitochondrial
Calcium-binding mitochondrial carrier protein Aralar1
Cytochrome b-c1 complex subunit Rieske, mitochondrial
Alpha-actinin-4
Aconitate hydratase, mitochondrial
Sideroflexin-3
Clathrin coat assembly protein AP180
Voltage-dependent anion-selective channel protein 2
Proteasome subunit beta type-6
Peroxiredoxin-1
Small nuclear ribonucleoprotein D3
Cold-inducible RNA-binding protein
RNA-binding protein EWS
Vesicle-associated membrane protein-associated protein A
Metastasis-associated protein MTA2
Peptidyl-prolyl cis-trans isomerase FKBP1A
40S ribosomal protein S10
Triosephosphate isomerase
6-phosphogluconolactonase
Inositol (Myo)-1(Or 4)-monophosphatase 1
Phosducin
Eukaryotic initiation factor 4A-II
DNA-(apurinic or apyrimidinic site) lyase
Heterogeneous nuclear ribonucleoprotein F
Control 2
Control 1
Control 5
Control 3
ONC 2
ONC 1
ONC 4
ONC 5
NMDA 1
NMDA 6
NMDA 3
NMDA 5
2.0
1.8
1.6
1.4
1.2
1.0
0.8
0.6
0.4
0.2
0.0
-0.2
-0.4
-0.6
-0.8
-1.0
-1.2
-1.4
-1.6
-1.8
-2.0
B
Control
NMDA
ONC
Cycs
β-actin
C
Cycs
**
**
Mean Density (A.U.)
1.5
1.0
0.5
0.0
Control
NMDA
ONC

UniProtKB Names	Acc#	Fold(NMDA/C)
NADH dehydrogenase [ubiquinone] 1 alpha subcomplex subunit 12	Q7TMF3	3.20
40S ribosomal protein S10	P63325	3.20
Peptidyl-prolyl cis-trans isomerase FKBP1A	P26883	2.93
Selenium-binding protein 1	P17563	2.68
SUMO-activating enzyme subunit 1	Q9R1T2	2.55
Peptidyl-prolyl cis-trans isomerase FKBP4	P30416	2.32
Probable ATP-dependent RNA helicase DDX28	Q9CWT6	2.28
Translationally-controlled tumor protein	P63028	2.27
Metastasis-associated protein MTA2	Q9R190	2.24
60S ribosomal protein L35a	O55142	2.08
Proteasome subunit alpha type-7	Q9Z2U0	2.07
6-phosphogluconolactonase	Q9CQ60	2.06
High mobility group protein HMG-I/HMG-Y	P17095	2.04
Plasminogen activator inhibitor 1 RNA-binding protein	Q9CY58	2.03
Phosducin	Q9QW08	1.98
ATP-dependent RNA helicase DDX1	Q91VR5	1.92
Eukaryotic translation initiation factor 4B	Q8BGD9	1.90
DnaJ homolog subfamily C member 8	Q6NZB0	1.83
ADP-ribosylation factor-like protein 3	Q9WUL7	1.82
Hypoxanthine-guanine phosphoribosyltransferase	P00493	1.81
OTU domain-containing protein 7A	Q8R554	1.80
Histone deacetylase complex subunit SAP18	O55128	1.77
Cytosolic non-specific dipeptidase	Q9D1A2	1.76
High mobility group protein B3	O54879	1.75
Actin-related protein 2/3 complex subunit 3	Q9JM76	1.73
Inositol (Myo)-1(Or 4)-monophosphatase 1	Q924B0	1.72
DNA-(apurinic or apyrimidinic site) lyase	P28352	1.72
Ras GTPase-activating protein 4	Q6PFQ7	1.68
Splicing factor 3A subunit 3	Q9D554	1.67
Lactoylglutathione lyase	Q9CPU0	1.62
Cold-inducible RNA-binding protein	P60824	1.61
Eukaryotic initiation factor 4A-II	E9Q561	1.59
Ribosomal protein S23	Q497E1	1.59
Inositol polyphosphate 1-phosphatase	P49442	1.57
Guanylate kinase	Q64520	1.55
Prostaglandin E synthase 3	Q9R0Q7	1.53
Elongation factor 1-beta	O70251	1.53
RNA-binding motif protein, X chromosome	Q9WV02	1.52
Glutathione S-transferase P 1	P19157	1.51
Ribosomal protein S14	O70569	1.50
Sodium/potassium-transporting ATPase subunit alpha-3	Q6PIC6	-1.51
Sodium/potassium-transporting ATPase subunit alpha-1	Q8VDN2	-1.54
Glycogen phosphorylase, brain form	Q8CI94	-1.55
Hsc70-interacting protein	Q99L47	-1.57
N(G),N(G)-dimethylarginine dimethylaminohydrolase 1	Q9CWS0	-1.60
Voltage-dependent anion-selective channel protein 2	Q60930	-1.61
Cytochrome b-c1 complex subunit 2, mitochondrial	Q9DB77	-1.62
Protein NipSnap homolog 2	O55126	-1.63

Very-long-chain 3-oxoacyl-CoA reductase	O70503	-1.63
Clathrin coat assembly protein AP180	Q61548	-1.63
Mitochondrial carrier homolog 2	Q791V5	-1.64
Thioredoxin-related transmembrane protein 1	Q8VBT0	-1.64
ATP synthase subunit d, mitochondrial	Q9DCX2	-1.64
Leucine-rich repeat-containing protein 59	Q922Q8	-1.67
Dihydrolipoyllysine-residue acetyltransferase component of pyruvate dehyd	Q8BMF4	-1.67
Cytoplasmic dynein 1 heavy chain 1	Q9JHU4	-1.68
Synaptogyrin-3	Q8R191	-1.69
Enoyl-CoA delta isomerase 1, mitochondrial	P42125	-1.71
MICOS complex subunit Mic60	Q8CAQ8	-1.71
Ras-related protein Rab-18	P35293	-1.71
Hexokinase-1	P17710	-1.74
Sideroflexin-5	Q925N0	-1.75
60 kDa heat shock protein, mitochondrial	P63038	-1.76
Aldose reductase	P45376	-1.77
Fumarate hydratase, mitochondrial	P97807	-1.79
Transportin-1	Q8BFY9	-1.79
Protein ERGIC-53	Q9D0F3	-1.79
MAGUK p55 subfamily member 2	Q9WV34	-1.79
Calcium-binding mitochondrial carrier protein Aralar1	Q8BH59	-1.80
Ribophorin	Q61833	-1.81
Dynamin-3	Q8BZ98	-1.83
Septin-7	O55131	-1.84
F-actin-capping protein subunit alpha-1	P47753	-1.84
Cytochrome c1, heme protein, mitochondrial	Q9D0M3	-1.87
Alpha-actinin-4	P57780	-1.90
Spectrin beta chain, non-erythrocytic 1	Q62261	-1.90
Succinyl-CoA ligase [ADP-forming] subunit beta, mitochondrial	Q9Z2I9	-1.91
Transforming protein RhoA	Q9QUI0	-1.93
Microtubule-associated protein 6	Q7TSJ2	-1.94
Spna2 protein	B9EKJ1	-1.94
Isocitrate dehydrogenase [NAD] subunit, mitochondrial	Q91VA7	-1.97
Protein disulfide-isomerase A4	P08003	-1.97
Protein NDRG2	Q9QYG0	-1.98
Brain acid soluble protein 1	Q91XV3	-1.98
Retinal dehydrogenase 1	P24549	-1.99
Cleavage and polyadenylation-specificity factor subunit 6	H3BJW3	-1.99
AP-1 complex subunit beta-1	O35643	-2.04
AP-2 complex subunit alpha-2	P17427	-2.05
Carbonic anhydrase 14	Q9WVT6	-2.06
40S ribosomal protein S3a	P97351	-2.07
S-formylglutathione hydrolase	Q9R0P3	-2.07
Pyruvate dehydrogenase E1 component subunit beta, mitochondrial	Q9D051	-2.18
60S acidic ribosomal protein P0	P14869	-2.21
Ornithine aminotransferase, mitochondrial	P29758	-2.23
Sideroflexin-3	Q91V61	-2.28
Septin-5	Q9Z2Q6	-2.31
CDGSH iron-sulfur domain-containing protein 1	Q91WS0	-2.33

Sodium- and chloride-dependent GABA transporter 3	P31650	-2.35
NADH dehydrogenase [ubiquinone] iron-sulfur protein 8, mitochondrial	Q8K3J1	-2.38
NADH dehydrogenase [ubiquinone] 1 alpha subcomplex subunit 6	Q9CQZ5	-2.47
Dihydrolipoyl dehydrogenase, mitochondrial	O08749	-2.48
Synaptoporin	Q8BGN8	-2.51
Mannose-P-dolichol utilization defect 1 protein	Q9R0Q9	-2.54
Catenin (Cadherin associated protein), alpha 1	Q6NV50	-2.55
Importin subunit beta-1	P70168	-2.59
Phosphatidate cytidylyltransferase 2	Q99L43	-2.60
V-type proton ATPase 116 kDa subunit a isoform 1	Q9Z1G4	-2.61
Cytochrome c, somatic	P62897	-2.65
Catenin beta-1	Q02248	-2.67
Cytochrome b-c1 complex subunit Rieske, mitochondrial	Q9CR68	-2.80
AP-2 complex subunit beta	Q9DBG3	-2.94
Pyridoxal kinase	Q8K183	-2.96
Neuronal membrane glycoprotein M6-a	P35802	-3.74

Ingenuity Canonical Pathways	-log(p-va	z-score	Molecules
Neutrophil degranulation	4.2	-2.5	AP2A2,ATP6V0A1,DYNC1H1,GSTP1,KPNB1,PDXK,PYGB,RAB18,RHOA,SPTAN1
MHC class II antigen presentation	3.5	-2.2	AP1B1,AP2A2,CAPZA1,DNM3,DYNC1H1
Sertoli Cell-Sertoli Cell Junction Signaling	2.3	-2.2	ACTN4,CTNNA1,CTNNB1,SPTAN1,SPTBN1
Oxidative Phosphorylation	7.3	-2.1	ATP5PD,CYC1,CYCS,NDUFA12,NDUFA6,NDUFS8,UQCRC2,UQCRFS1
Electron transport, ATP synthesis, and heat production by uncoupling proteins	6.9	-2.1	ATP5PD,CYC1,CYCS,NDUFA12,NDUFA6,NDUFS8,UQCRC2,UQCRFS1
TCA Cycle II (Eukaryotic)	5.5	-2.0	DLD,FH,IDH3B,SUCLA2
Signaling by Retinoic Acid	4.3	-2.0	ALDH1A1,DLAT,DLD,PDHB
COPI-mediated anterograde transport	2.9	-2.0	CAPZA1,DYNC1H1,SPTAN1,SPTBN1
L1CAM interactions	2.6	-2.0	AP2A2,DNM3,SPTAN1,SPTBN1
Leukocyte Extravasation Signaling	1.9	-2.0	ACTN4,CTNNA1,CTNNB1,RHOA
The citric acid (TCA) cycle and respiratory electron transport	8.2	-1.9	DLAT,DLD,FH,GLO1,IDH3B,PDHB,SUCLA2
Neutrophil Extracellular Trap Signaling Pathway	2.6	-1.9	CYC1,NDUFA12,NDUFA6,NDUFS8,UQCRC2,UQCRFS1,VDAC2
RHO GTPase cycle	2.3	-1.9	BASP1,LMAN1,NIPSNAP2,RBMX,RHOA,SPTAN1,SPTBN1
Clathrin-mediated endocytosis	3.5	-1.3	AP2A2,Ap2b1,ARPC3,DNM3,SNAP91
EPH-Ephrin signaling	3.0	-1.0	AP2A2,Ap2b1,ARPC3,RHOA
RHOA Signaling	2.6	-1.0	ARPC3,RHOA,SEPTIN5,SEPTIN7
Estrogen Receptor Signaling	2.6	-1.0	CYC1,NDUFA12,NDUFA6,NDUFS8,RHOA,UQCRC2,UQCRFS1
Epithelial Adherens Junction Signaling	2.2	-1.0	ARPC3,CTNNA1,CTNNB1,RHOA
Mitotic Metaphase and Anaphase	1.6	-1.0	DYNC1H1,KPNB1,PSMA7,TNPO1
Signaling by Rho Family GTPases	1.5	-1.0	ARPC3,RHOA,SEPTIN5,SEPTIN7
Insulin Secretion Signaling Pathway	1.4	-1.0	DLAT,DLD,EIF4A2,PDHB
Autism Signaling Pathway	1.3	-1.0	ALDH1A1,CTNNB1,DLD,HPRT1
Eukaryotic Translation Termination	3.0	1.0	RPL35A,RPLP0,RPS10,RPS23
Response of EIF2AK4 (GCN2) to amino acid deficiency	2.9	1.0	RPL35A,RPLP0,RPS10,RPS23
Selenoamino acid metabolism	2.8	1.0	RPL35A,RPLP0,RPS10,RPS23
Nonsense-Mediated Decay (NMD)	2.7	1.0	RPL35A,RPLP0,RPS10,RPS23
Major pathway of rRNA processing in the nucleolus and cytosol	2.0	1.0	RPL35A,RPLP0,RPS10,RPS23
Eukaryotic Translation Elongation	4.1	1.3	EEF1B2,RPL35A,RPLP0,RPS10,RPS23
Processing of Capped Intron-Containing Pre-mRNA	2.0	1.3	CPSF6,DNAJC8,RBMX,SAP18,SF3A3
Eukaryotic Translation Initiation	4.7	1.6	EIF4A2,EIF4B,RPL35A,RPLP0,RPS10,RPS23
Macrophage Classical Activation Signaling Pathway	2.0	2.0	DLAT,DLD,PDHB,UQCRC2

UniProtKB Names	Acc#	Fold(Onc/C)
Splicing factor 3A subunit 1	Q8K4Z5	2.62
CST complex subunit STN1	Q8K2X3	2.59
Stomatin-like protein 2, mitochondrial	Q99JB2	2.37
DnaJ homolog subfamily C member 8	Q6NZB0	2.05
Arginine and glutamate-rich protein 1	Q3UL36	1.99
Hepatoma-derived growth factor-related protein 2	Q3UMU9	1.95
Serine/arginine-rich splicing factor 6	Q3TWW8	1.91
Ddx3x protein	B9EKE9	1.90
Probable ATP-dependent RNA helicase DDX28	Q9CWT6	1.88
RNA-binding protein FUS	P56959	1.86
Proteasome subunit beta type-2	Q9R1P3	1.86
AP-3 complex subunit beta-2	Q9JME5	1.86
von Willebrand factor A domain-containing protein 8	Q8CC88	1.83
Transmembrane protein 33	Q9CR67	1.77
Soluble lamin-associated protein of 75 kDa	Q5XG69	1.66
Proteasome subunit alpha type	Q9DCD8	1.66
High mobility group protein B3	O54879	1.63
DNA-(apurinic or apyrimidinic site) lyase	P28352	1.55
Sodium-coupled neutral amino acid transporter 3	Q9DCP2	1.55
C2 domain-containing protein 2-like	Q80X80	1.54
Mitochondrial Rho GTPase 1	Q8BG51	1.54
Inosine-5'-monophosphate dehydrogenase 1	P50096	1.54
Clathrin light chain A	O08585	1.51
Translationally-controlled tumor protein	P63028	1.49
Fumarate hydratase, mitochondrial	P97807	-1.49
Glycogen phosphorylase, muscle form	Q9WUB3	-1.50
Actin-related protein 3	Q99JY9	-1.50
Synaptotagmin-1	P46096	-1.50
Sideroflexin-3	Q91V61	-1.50
Proteasome subunit beta type-6	Q60692	-1.52
ATP-dependent 6-phosphofructokinase, liver type	P12382	-1.53
NADH dehydrogenase [ubiquinone] 1 alpha subcomplex subunit 7	Q9Z1P6	-1.53
Dynactin subunit 2	Q99KJ8	-1.54
T-complex protein 1 subunit alpha	P11983	-1.55
High mobility group protein HMG-I/HMG-Y	P17095	-1.56
Brevican core protein	Q61361	-1.56
Proteasome subunit alpha type-6	Q9QUM9	-1.57
Hippocalcin-like protein 4	Q8BGZ1	-1.57
RuvB-like 2	Q9WTM5	-1.58
Protein kinase, cAMP dependent regulatory, type II alpha	Q8K1M3	-1.59
Clathrin coat assembly protein AP180	Q61548	-1.61
Glutaminase kidney isoform, mitochondrial	D3Z7P3	-1.62
Cytochrome c oxidase subunit 7C, mitochondrial	P17665	-1.70
Carbonic anhydrase 14	Q9WVT6	-1.71
Dynamin-1	P39053	-1.73
Protein disulfide-isomerase A3	P27773	-1.74

Beta-centractin	Q8R5C5	-1.74
Phosphoglucomutase-1	Q9D0F9	-1.74
SH3 domain-binding glutamic acid-rich-like protein 3	Q91VW3	-1.75
NADH dehydrogenase [ubiquinone] 1 subunit C2	Q9CQ54	-1.76
Cell cycle and apoptosis regulator protein 2	Q8VDP4	-1.77
Cofilin-1	P18760	-1.77
Isocitrate dehydrogenase [NAD] subunit, mitochondrial	Q91VA7	-1.77
Mitochondrial 2-oxoglutarate/malate carrier protein	Q9CR62	-1.78
Ras-related protein Rab-18	P35293	-1.78
Kras protein	Q5J7N1	-1.78
AP-1 complex subunit beta-1	O35643	-1.78
Enoyl-CoA hydratase, mitochondrial	Q8BH95	-1.81
Transforming protein RhoA	Q9QUI0	-1.81
Prohibitin	P67778	-1.82
Transportin-1	Q8BFY9	-1.84
40S ribosomal protein S12	P63323	-1.84
Cytochrome b-c1 complex subunit Rieske, mitochondrial	Q9CR68	-1.85
Ankyrin-2	Q8C8R3	-1.87
NADH dehydrogenase [ubiquinone] 1 beta subcomplex subunit 10	Q9DCS9	-1.94
26S proteasome non-ATPase regulatory subunit 2	Q8VDM4	-1.96
U2 small nuclear ribonucleoprotein A'	P57784	-1.98
Dynamin-3	Q8BZ98	-2.00
Tubby-related protein 1	Q9Z273	-2.02
Mitochondrial import receptor subunit TOM70	Q9CZW5	-2.04
Pyridoxal phosphate phosphatase	P60487	-2.07
Protein NipSnap homolog 2	O55126	-2.13
Cold-inducible RNA-binding protein	P60824	-2.14
ATP-dependent 6-phosphofructokinase, muscle type	P47857	-2.15
RNA-binding protein EWS	Q61545	-2.18
Glycogen phosphorylase, brain form	Q8CI94	-2.19
Brain acid soluble protein 1	Q91XV3	-2.20
Galectin-related protein	Q8VED9	-2.21
Ornithine aminotransferase, mitochondrial	P29758	-2.22
CDGSH iron-sulfur domain-containing protein 1	Q91WS0	-2.27
Putative adenosylhomocysteinase 3	Q68FL4	-2.28
Synaptic vesicle glycoprotein 2B	Q8BG39	-2.28
Cytosolic acyl coenzyme A thioester hydrolase	Q91V12	-2.32
Krt2 protein	B2RTP7	-2.33
Moesin	P26041	-2.34
Rab GDP dissociation inhibitor beta	Q61598	-2.44
Microtubule-associated protein 6	Q7TSJ2	-2.46
NADH dehydrogenase [ubiquinone] 1 alpha subcomplex subunit 8	Q9DCJ5	-2.51
Catenin (Cadherin associated protein), alpha 1	Q6NV50	-2.51
Fas apoptotic inhibitory molecule 1	Q9WUD8	-2.53
N(G),N(G)-dimethylarginine dimethylaminohydrolase 1	Q9CWS0	-2.59
Septin-7	O55131	-2.59
Sodium- and chloride-dependent GABA transporter 3	P31650	-2.64

Secretagogin	Q91WD9	-2.67
Isocitrate dehydrogenase [NAD] subunit gamma 1, mitochondrial	P70404	-2.67
UMP-CMP kinase	Q9DBP5	-2.69
Catenin beta-1	Q02248	-2.72
Glutathione S-transferase Mu 1	P10649	-3.01
V-type proton ATPase 116 kDa subunit a isoform 1	Q9Z1G4	-3.01
Vesicle-associated membrane protein-associated protein A	Q9WV55	-3.25
AP-2 complex subunit beta	Q9DBG3	-3.38
Protein disulfide-isomerase A4	P08003	-3.57
Dihydrolipoyl dehydrogenase, mitochondrial	O08749	-3.67
Cytochrome c, somatic	P62897	-3.88
Importin subunit beta-1	P70168	-4.22

Ingenuity Canonical Pathways	-log(p-value)	z-score	Molecules
Neutrophil degranulation	7.8	-2.7	ACTR1B,ATP6V0A1,DDX3X,GDI2,IMPDH1,KPNB1,NDUFC2,PFKL,PGM1,PSMD2,PYGB,RAB18,RHOA,VAPA
Electron transport, ATP synthesis, and heat production by uncoupling proteins	4.7	-2.4	CYCS,NDUFA7,NDUFA8,NDUFB10,NDUFC2,UQCRFS1
Eicosanoid Signaling	2.9	-2.4	AP1B1,CTNNB1,KRAS,PDIA3,PRKAR2A,RHOA
Neutrophil Extracellular Trap Signaling Pathway	2.1	-2.4	NDUFA7,NDUFA8,NDUFB10,PDIA3,TOMM70,UQCRFS1
Oxidative Phosphorylation	3.9	-2.2	CYCS,NDUFA7,NDUFA8,NDUFB10,UQCRFS1
RHOA Signaling	3.7	-2.2	ACTR3,CFL1,MSN,RHOA,SEPTIN7
TCA Cycle II (Eukaryotic)	5.6	-2.0	DLD,FH,IDH3B,IDH3G
The citric acid (TCA) cycle and respiratory electron transport	4.0	-2.0	DLD,FH,IDH3B,IDH3G
Signaling by VEGF	2.9	-2.0	CTNNA1,CTNNB1,KRAS,RHOA
RAC Signaling	2.5	-2.0	ACTR3,CFL1,KRAS,RHOA
Opioid Signaling Pathway	2.1	-2.0	Ap2b1,CLTA,CTNNB1,KRAS,PRKAR2A
Leukocyte Extravasation Signaling	2.0	-2.0	CTNNA1,CTNNB1,MSN,RHOA
Ephrin Receptor Signaling	1.9	-2.0	ACTR3,CFL1,KRAS,RHOA
Pancreatic Secretion Signaling Pathway	1.7	-2.0	CA14,PDIA3,PRKAR2A,RHOA
Clathrin-mediated endocytosis	5.8	-1.9	ACTR3,Ap2b1,CLTA,DNM1,DNM3,SNAP91,SYT1
EPH-Ephrin signaling	5.5	-1.6	ACTR3,Ap2b1,CFL1,CLTA,DNM1,RHOA
MHC class II antigen presentation	4.8	-1.6	ACTR1B,AP1B1,CLTA,DCTN2,DNM1,DNM3
Protein Kinase A Signaling	2.7	-1.6	APEX1,CTNNB1,PDIA3,PRKAR2A,PYGB,PYGM,RHOA
Cardiac Hypertrophy Signaling (Enhanced)	1.5	-1.6	APEX1,CTNNB1,KRAS,PDIA3,PRKAR2A,RHOA
Signaling by NTRK1 (TRKA)	4.6	-1.3	CLTA,DNM1,DNM3,KRAS,RHOA
L1CAM interactions	3.7	-1.3	Ank2,CLTA,DNM1,DNM3,MSN
Glioblastoma Multiforme Signaling	3.1	-1.3	CTNNB1,KRAS,PDIA3,RHOA,RHOT1
Signaling by Rho Family GTPases	3.0	-1.3	ACTR3,CFL1,MSN,RHOA,RHOT1,SEPTIN7
Actin Cytoskeleton Signaling	2.4	-1.3	ACTR3,CFL1,KRAS,MSN,RHOA
Cardiac Hypertrophy Signaling	2.3	-1.3	KRAS,PDIA3,PRKAR2A,RHOA,RHOT1
Colorectal Cancer Metastasis Signaling	2.2	-1.3	CTNNB1,KRAS,PRKAR2A,RHOA,RHOT1
Serotonin Receptor Signaling	1.3	-1.3	KRAS,PDIA3,PRKAR2A,RHOA,RHOT1
Transcriptional regulation by RUNX3	6.7	-1.1	CTNNB1,KRAS,PSMA3,PSMA6,PSMB2,PSMB6,PSMD2
Signaling by ROBO receptors	6.2	-1.1	PRKAR2A,PSMA3,PSMA6,PSMB2,PSMB6,PSMD2,RHOA
Synaptogenesis Signaling Pathway	4.2	-1.1	ACTR3,Ap2b1,CFL1,CTNNB1,KRAS,PRKAR2A,RHOA,SYT1
Mitotic Metaphase and Anaphase	4.1	-1.1	KPNB1,PSMA3,PSMA6,PSMB2,PSMB6,PSMD2,TNPO1
RAF/MAP kinase cascade	3.9	-1.1	KRAS,PHB1,PSMA3,PSMA6,PSMB2,PSMB6,PSMD2
Chaperone Mediated Autophagy Signaling Pathway	1.7	-1.1	ATP6V0A1,DDX3X,PSMA3,PSMA6,PSMB2,PSMB6,TPT1
Gene and protein expression by JAK-STAT signaling after IL-12 stimulation	4.7	-1.0	CFL1,MSN,SNRPA1,TCP1
Actin Nucleation by ARP-WASP Complex	3.2	-1.0	ACTR3,KRAS,RHOA,RHOT1
Cargo recognition for clathrin-mediated endocytosis	2.9	-1.0	Ap2b1,CLTA,SNAP91,SYT1
ILK Signaling	2.0	-1.0	CFL1,CTNNB1,RHOA,RHOT1
Integrin Signaling	1.9	-1.0	ACTR3,KRAS,RHOA,RHOT1
Thrombin Signaling	1.8	-1.0	KRAS,PDIA3,RHOA,RHOT1
Docosahexaenoic Acid (DHA) Signaling	1.6	-1.0	CYCS,PDIA3,PRKAR2A,SYT1
Autism Signaling Pathway	1.4	-1.0	CTNNB1,DLD,KRAS,PRKAR2A
Glutaminergic Receptor Signaling Pathway (Enhanced)	1.3	-1.0	GLS,PDIA3,PRKAR2A,SLC38A3
Gap Junction Signaling	1.3	-1.0	CTNNB1,KRAS,PDIA3,PRKAR2A
Granzyme A Signaling	3.5	1.0	APEX1,NDUFA7,NDUFA8,NDUFB10
Processing of Capped Intron-Containing Pre-mRNA	1.5	1.0	DNAJC8,SF3A1,SNRPA1,SRSF6
Sirtuin Signaling Pathway	5.3	1.6	APEX1,GLS,NDUFA7,NDUFA8,NDUFB10,PFKM,SF3A1,TOMM70,UQCRFS1
Mitochondrial Dysfunction	4.7	1.7	CYCS,DLD,NDUFA7,NDUFA8,NDUFB10,PRKAR2A,RHOT1,TOMM70,UQCRFS1

UniProtKB Names	Acc#	Fold(NMDA/C)	Fold(Onc/C)
Importin subunit beta-1	P70168	-2.59	-4.22
Cytochrome c, somatic	P62897	-2.65	-3.88
Dihydrolipoyl dehydrogenase, mitochondrial	O08749	-2.48	-3.67
Protein disulfide-isomerase A4	P08003	-1.97	-3.57
AP-2 complex subunit beta	Q9DBG3	-2.94	-3.38
V-type proton ATPase 116 kDa subunit a isoform 1	Q9Z1G4	-2.61	-3.01
Catenin beta-1	Q02248	-2.67	-2.72
Sodium- and chloride-dependent GABA transporter 3	P31650	-2.35	-2.64
Septin-7	O55131	-1.84	-2.59
N(G),N(G)-dimethylarginine dimethylaminohydrolase 1	Q9CWS0	-1.60	-2.59
Catenin (Cadherin associated protein), alpha 1	Q6NV50	-2.55	-2.51
Microtubule-associated protein 6	Q7TSJ2	-1.94	-2.46
CDGSH iron-sulfur domain-containing protein 1	Q91WS0	-2.33	-2.27
Ornithine aminotransferase, mitochondrial	P29758	-2.23	-2.22
Brain acid soluble protein 1	Q91XV3	-1.98	-2.20
Glycogen phosphorylase, brain form	Q8CI94	-1.55	-2.19
Cold-inducible RNA-binding protein	P60824	1.61	-2.14
Protein NipSnap homolog 2	O55126	-1.63	-2.13
Dynamin-3	Q8BZ98	-1.83	-2.00
Cytochrome b-c1 complex subunit Rieske, mitochondrial	Q9CR68	-2.80	-1.85
Transportin-1	Q8BFY9	-1.79	-1.84
Transforming protein RhoA	Q9QUI0	-1.93	-1.81
AP-1 complex subunit beta-1	O35643	-2.04	-1.78
Ras-related protein Rab-18	P35293	-1.71	-1.78
Isocitrate dehydrogenase [NAD] subunit, mitochondrial	Q91VA7	-1.97	-1.77
Carbonic anhydrase 14	Q9WVT6	-2.06	-1.71
Clathrin coat assembly protein AP180	Q61548	-1.63	-1.61
High mobility group protein HMG-I/HMG-Y	P17095	2.04	-1.56
Sideroflexin-3	Q91V61	-2.28	-1.50
Fumarate hydratase, mitochondrial	P97807	-1.79	-1.49
Translationally-controlled tumor protein	P63028	2.27	1.49
DNA-(apurinic or apyrimidinic site) lyase	P28352	1.72	1.55
High mobility group protein B3	O54879	1.75	1.63
Probable ATP-dependent RNA helicase DDX28	Q9CWT6	2.28	1.88
DnaJ homolog subfamily C member 8	Q6NZB0	1.83	2.05